

Synthesis, crystal structure and mono-dimensional thallium ion conduction of $\text{TiFe}_{0.22}\text{Al}_{0.78}\text{As}_2\text{O}_7$

Najoua Ouerfelli^a, Abderrahmen Guesmi^{a,*}, Daniele Mazza^b, Adel Madani^c, Mohamed Faouzi Zid^a, Ahmed Driss^a

^aLaboratoire de Matériaux et Cristallochimie, Faculté des Sciences, El Manar, 2092 Tunis, Tunisia

^bDipartimento di Scienza dei Materiali e Ingegneria Chimica, Politecnico di Torino, Corso Duca degli Abruzzi 24, 10129 Torino, Italy

^cLaboratoire de Physique des Matériaux, Faculté des Sciences de Bizerte, 7021 Bizerte, Tunisia

Received 9 November 2006; received in revised form 6 January 2007; accepted 7 January 2007

Available online 26 January 2007

Abstract

A new solid solution $\text{TiFe}_{0.22}\text{Al}_{0.78}\text{As}_2\text{O}_7$ has been synthesized by a solid-state reaction. The structure of the title compound has been determined from a single-crystal X-ray diffraction and refined to final values of the reliability factors: $R(F^2) = 0.030$ and $wR(F^2) = 0.081$ for 1343 independent reflections with $I > 2\sigma(I)$. It crystallizes in the triclinic space group $P-1$, with $a = 6.296(2)\text{ \AA}$, $b = 6.397(2)\text{ \AA}$, $c = 8.242(2)\text{ \AA}$, $\alpha = 96.74(2)^\circ$, $\beta = 103.78(2)^\circ$, $\gamma = 102.99(3)^\circ$, $V = 309.0(2)\text{ \AA}^3$ and $Z = 2$. The structure can be described as a three-dimensional framework containing $(\text{Fe/Al})\text{O}_6$ octahedra connected through As_2O_7 groups. The metallic units and diarsenate groups share oxygen corners to form a three-dimensional framework with interconnected tunnels parallel to the a , b and c directions, where Ti^+ cations are located. The ionic conductivity measurements are performed on pellets of the polycrystalline powder. At 683 K, The conductivity value is $5.23 \times 10^{-6}\text{ S cm}^{-1}$ and the ionic jump activation energy is 0.656 eV. The bond valence analysis reveals that the ionic conductivity is ensured by Ti^+ along the [001] direction.

© 2007 Elsevier Inc. All rights reserved.

Keywords: X-ray diffraction; Crystal structure; ECoN; Ionic conductivity; Bond valence analysis; Infrared spectroscopy

1. Introduction

Many diphosphates with the general formula $\text{A}^{\text{I}}\text{M}^{\text{III}}\text{P}_2\text{O}_7$ have been extensively studied during the last years [1]. It was revealed that the phosphates showed a variety of structures composed of MO_6 octahedra and P_2O_7 groups. Some of these compounds have tunnel or cage structures, in which alkali ions reside and therefore are good candidates for new ionic conductors. Some of them are largely developed in catalysis [2]. Compared to the rich chemistry of the iron diphosphates, iron diarsenates studies are rare in the literature. Only three iron diarsenates, $\text{NaFeAs}_2\text{O}_7$ [3], $\text{AgFeAs}_2\text{O}_7$ [3] and $\text{LiFeAs}_2\text{O}_7$ [4], have been studied in single-crystal form. The aim of this work is to elucidate the crystal structure of the arsenate

$\text{TiFe}_{0.22}\text{Al}_{0.78}\text{As}_2\text{O}_7$ and to examine the relationship between the structure and the thallium ionic conductivity.

2. Experimental

Single crystals of the title compound were obtained from a mixture of Ti_2CO_3 , $M(\text{NO}_3)_3 \cdot 9\text{H}_2\text{O}$, ($M = \text{Fe, Al}$) and H_3AsO_4 with a Ti:Fe:Al:As molar ratio of 1:0.1:0.9:2. The synthesis technique consists to completely dissolve the reagents in an aqueous solution. The mixture is slowly evaporated to total dryness and then placed in an alumina crucible. The calcinations of the dry residue are performed through three steps: first at 400 °C for 3 h, second heated to 700 °C for 3 h, the molten mixture is then cooled to 650 °C/12 h and finally slowly cooled to room temperature. The obtained green crystals were separated from the excess flux by washing the product in boiling water.

The Fourier transform infrared (FTIR) measurements were performed at room temperature, on a Perkin-Elmer

*Corresponding author. Fax: +216 71 885 008.

E-mail addresses: abderrahman.guesmi@ipeim.rnu.tn, gabderrahmen@yahoo.fr (A. Guesmi).

FT-IR Paragon 1000 PC spectrometer over the 1400–400 cm^{−1} region, in a KBr pellet.

Impedance measurements were carried out in a Hewlett-Packard 4192-A automatic bridge monitored by a HP microcomputer. The frequency range was 5 Hz–13 MHz. Pellets of 13 mm diameter and 0.6 mm thickness were prepared by pressing the powder sample at 10 tonnes. Then the pellets were sintered at 600 °C for 24 h. Silver electrodes were painted in the two faces of the pellets with a silver paste, and then the painted pellets were heated at 300 °C/1 h. The impedance measurements were carried out at steady-state temperatures on the pellets in still air.

3. Results and discussion

3.1. Structure determination

A suitable green single crystal with dimensions 0.144 × 0.114 × 0.108 mm³ was chosen for the structure determination and refinement. It was selected under a polarizing microscope and was mounted on a glass fibre. The crystal structure is determined from single-crystal X-ray diffraction data collected at room temperature using an Enraf-Nonius CAD-4 diffractometer with monochromated graphite MoK α radiation ($\lambda = 0.71069 \text{ \AA}$) [5]. The reflections were corrected for Lorentz and polarization effects; absorption correction was obtained via a psi-scan [6] and secondary extinction correction was applied too [7].

The crystal structure was solved and refined against F^2 in the space-group *P*-1 using the SHELX-97 [7,8] computer programs included in the WingX software package [9]. The iron, thallium and arsenic atoms were located and the remaining oxygen atoms were found from successive difference Fourier maps. Refinement of all atoms, except of aluminium led to $R = 0.0566$ and $wR = 0.1634$. Moreover, the M–O distances (position 2*i*) as well as the displacement parameters led us to consider that the (2*i*) position is occupied simultaneously by iron and aluminium. Besides, the semi-quantitative energy-dispersive spectroscopy (EDS) analysis of one of the green stick-like crystals obtained as mentioned above was performed with a JEOL-JSM 5400 scanning electron microscope; it revealed the presence of Tl, As, Fe, Al and O elements. The refinement of the occupancy factors of the two metals was then performed leading to 22% and 78% for Fe and Al, respectively, and to an improvement of the agreement factors: $R = 0.030$ and $wR = 0.081$; the corresponding formula is thus $\text{TiFe}_{0.22}\text{Al}_{0.78}\text{As}_2\text{O}_7$. Both bond valence model [10,11] and charge distribution analysis [12–14] show that the structure is well refined with satisfactory valences (V)/charges (Q) for all atoms (Table 3).

The crystallographic data and experimental conditions for intensity measurements and refinement are reported in Table 1. The atomic coordinates, fractional occupancies and isotropic displacement parameters are listed in Table 2. The main interatomic distances are given in Table 3.

Table 1

Summary of crystallographic data, recording conditions and structure refinement results for $\text{TiFe}_{0.22}\text{Al}_{0.78}\text{As}_2\text{O}_7$

Crystal data

Empirical formula	$\text{TiFe}_{0.22}\text{Al}_{0.78}\text{As}_2\text{O}_7$
Crystal system; space group	Triclinic; <i>P</i> -1
Unit cell dimensions	$a = 6.296(2) \text{ \AA}$, $b = 6.397(2) \text{ \AA}$, $c = 8.242(2) \text{ \AA}$, $\alpha = 96.74(2)^\circ$, $\beta = 103.78(2)^\circ$, $\gamma = 102.99(3)^\circ$
Volume; Z	308.98 (16) \AA^3 ; 2
Formula weight; ρ_{calc}	499.54 g mol ^{−1} ; 5.369 g cm ^{−3}
Cell parameters from 25 reflections	$9.75 \leq \theta \leq 17.88^\circ$
Absorption coefficient (μ)	36.389 mm ^{−1}
Crystal shape; color	Parallelepiped; green
Crystal size	0.144 × 0.114 × 0.108 mm ³

Data collection

Diffractometer	Enraf-Nonius CAD-4
Wavelength; temperature	$\lambda_{\text{Mo } K\alpha} = 0.71069 \text{ \AA}$; 298(2) K
Theta range for data collection	$2.59 \leq \theta \leq 26.97^\circ$
Limiting indices	$-8 \leq h \leq 6$; $-8 \leq k \leq 8$; $0 \leq l \leq 10$
Scan mode	$\omega/2\theta$
Absorption correction; T_{min} ; T_{max}	psi-scan; 0.5297; 0.9987
Standards; frequency (min); decay (%)	2; 120; 1
Reflections collected	1399
Independent reflections	1316 [$R_{\text{int.}} = 0.0241$]
Observed reflections [$I > 2\sigma(I)$]	1200

Refinement

Refinement method	Full-matrix least-squares on F^2
Final R indices [$I > 2\sigma(I)$]	$R = 0.030$; $wR = 0.081$
Reflections; parameters	1316; 106
$\Delta\rho_{\text{max}}$; $\Delta\rho_{\text{min}}$ (e.Å ^{−3})	2.278; −1.593
Extinction coefficient	0.010(1)
Goodness of fit (S)	1.14

The structural figures were carried out with Diamond 2.1 supplied by Crystal Impact [15].

3.2. Structure description and discussion

The title compound is isostructural to $\text{RbAlAs}_2\text{O}_7$ [16], KAlAs_2O_7 [17] and KGaAs_2O_7 [18]. The structure depicted in Fig. 1 can be described as a three-dimensional framework of $[\text{Fe}_{0.22}\text{Al}_{0.78}\text{As}_2\text{O}_7]^-$ anions, which are built up from corner-sharing MO_6 octahedra ($M = \text{Fe}_{0.22}\text{Al}_{0.78}$) and As_2O_7 groups. The metallic octahedron shares its six corners with five diarsenate groups; the As_2O_7 anion shares all its six corners with five octahedra; the interconnection between the polyhedra results in centrosymmetric $M\text{As}_2\text{O}_{11}$ units (Fig. 2). The framework can also be described as been formed from polyhedral parallel layers, as in many isoformula compounds [3,4,15–19]. It define interconnected tunnels parallel to the cell directions, where Tl^+ cations house.

Iron and aluminium cations occupy the same (2*i*) crystallographic site with occupancy rates of 0.22 and 0.78, respectively. These cations are coordinated by oxygen atoms in an octahedral coordination. The effective coordination number (ECoN) [12–14] of 5.992 shows that

Table 2

Atomic coordinates, fractional occupancies and equivalent isotropic thermal factors in $\text{TiFe}_{0.22}\text{Al}_{0.78}\text{As}_2\text{O}_7$

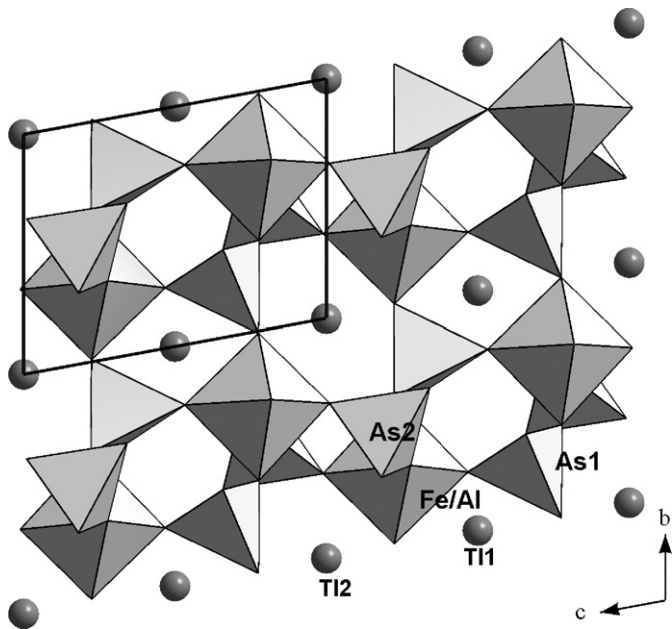
Atom	Position	<i>x</i>	<i>y</i>	<i>z</i>	Occupancy	U_{eq} (\AA^2)
As1	$2i$	0.48872 (12)	0.24234 (11)	0.33479 (8)	1	0.0034 (2)
As2	$2i$	0.17631 (12)	0.47112 (11)	0.81196 (8)	1	0.0035 (2)
Fe	$2i$	0.3753 (3)	0.6869 (3)	0.2273 (2)	0.222 (11)	0.0034 (6)
Al	$2i$	0.3753 (3)	0.6869 (3)	0.2273 (2)	0.778 (11)	0.0034 (6)
Tl1	$1b$	0	0	0.5	1	0.0333 (2)
Tl2	$1a$	0	0	0	1	0.0408 (2)
O1	$2i$	0.4223 (10)	-0.0089 (8)	0.2250 (7)	1	0.0106 (11)
O2	$2i$	0.4659 (9)	0.2516 (9)	0.5330 (6)	1	0.0091 (10)
O3	$2i$	0.3242 (9)	0.3769 (8)	0.2229 (6)	1	0.0068 (10)
O4	$2i$	0.2293 (9)	-0.3664 (8)	0.650 (6)	1	0.0090 (10)
O5	$2i$	0.2214 (9)	0.6447 (8)	0.9896 (6)	1	0.0080 (10)
O6	$2i$	-0.0908 (9)	0.3244 (8)	0.7230 (6)	1	0.0074 (10)
O7	$2i$	0.6624 (9)	0.7050 (8)	0.1825 (7)	1	0.0083 (10)

 U_{eq} is defined as one-third of the trace of the orthogonalized U_{ij} tensor.

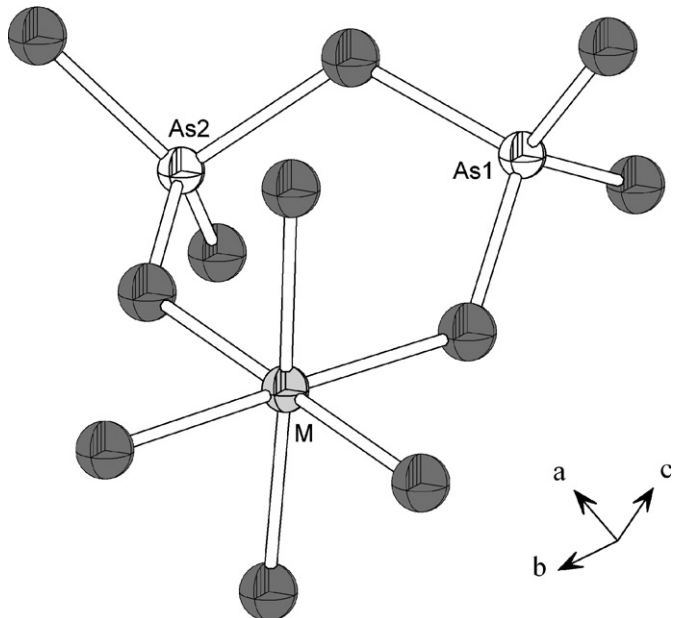
Table 3

Bond valence computation (V) and charge distribution analysis (Q) for $\text{TiFe}_{0.22}\text{Al}_{0.78}\text{As}_2\text{O}_7$

Fe/Al	As1	As2	Tl1	Tl2	O1	O2	O2	O4	O5	O6	O7
V	3.13	4.89	4.89	0.89	1.07	-2.04	-1.94	-1.95	-1.93	-2.04	-2.03
Q	2.98	5.07	4.95	0.99	0.99	-2.04	-1.96	-1.95	-1.94	-2.04	-2.06

Fig. 1. Polyhedral representation of $\text{TiFe}_{0.22}\text{Al}_{0.78}\text{As}_2\text{O}_7$ structure viewed along the *a*-axis showing the tunnels along the [100] direction.

the overall degree of distortion of the octahedron with respect to its regular counterpart is very limited. This comes from the fact that the longest distance and the smallest one differs only from 0.038 \AA ; furthermore, the arithmetic and weighted average distances [12–14] are two equals to 1.919 \AA .

Fig. 2. Perspective view of $M\text{As}_2\text{O}_{11}$ unit, $M = \text{Fe}_{0.22}\text{Al}_{0.78}$.

The diarsenate group As_2O_7 is formed by two slightly distorted As1O_4 and As2O_4 tetrahedra. The ECoNs are $\text{ECoN(As1)} = 3.934$, $\text{ECoN(As2)} = 3.903$; the arithmetic and weighted average distances for As1O_4 and As2O_4 are $\langle \text{As1-O} \rangle = 1.692 \text{ \AA}$ and $\langle \text{As2-O} \rangle = 1.693 \text{ \AA}$ and $\langle \text{As1-O} \rangle = 1.686 \text{ \AA}$ and $\langle \text{As2-O} \rangle = 1.686 \text{ \AA}$,

respectively; the overall degree of distortion is limited. The diarsenate group has a nearly eclipsed conformation with a torsion angle $O3-As1-As2-O7 = 26.97(2)^\circ$. The $O-As-O$ bond angles are between $106.9(3)^\circ$ and $113.7(3)^\circ$ and between $102.6(2)^\circ$ and $116.7(3)^\circ$ for As(1) and As(2), respectively. The $As1-O4-As2$ angle of $119.27(2)^\circ$ compares well with the corresponding angle in the literature.

There are two independent thallium positions in the unit cell. They are 4.094 \AA apart along $[001]$ direction. If we consider only $Tl-O$ distances less than 3.5 \AA . The $Tl(1)$ and $Tl(2)$ cations are surrounded by eight and ten oxygen atoms, with distances ranging from $2.854(5)$ to $3.261(5)\text{ \AA}$ and from $2.873(6)$ to $3.297(5)\text{ \AA}$ (Table 4), respectively, forming irregular coordination polyhedra, as often occurs with this cation. The stereochemical activity of the lone pair $6s^2$ of Tl^+ appears to be absent.

3.3. Infrared spectroscopy

The IR spectrum displays the typical bands of the diarsenate group whose main characteristic bands are v_s and v_{as} $As-O-As$ vibrations. The peaks at $586/773\text{ cm}^{-1}$ are attributed to symmetric v_s and asymmetric (v_{as}) modes of the As_2O_7 group, respectively (Fig. 3). The $As-O$ stretching and $O-As-O$ bending vibrational associated with AsO_4 tetrahedra are shown at 929, 877, 472 and

Table 4

Analysis of the coordination polyhedra for $TlFe_{0.22}Al_{0.78}As_2O_7$: main interatomic distances (\AA), classical coordination numbers (CN) and effective coordination numbers (ECoN)

	CN/ECoN: 4/	(Fe/Al)	CN/ECoN: 6/
As1 tetrahedron	3.934	octahedron	5.992
As1–O1	1.659 (5)	(Fe/Al)–O1 ⁱⁱⁱ	1.904 (5)
As1–O2	1.669 (5)	(Fe/Al)–O7	1.911 (6)
As1–O3	1.672 (5)	(Fe/Al)–O6 ^{iv}	1.919 (5)
As1–O4 ⁱ	1.760 (5)	(Fe/Al)–O5 ^v	1.924 (5)
		(Fe/Al)–O3	1.931 (5)
As2 tetrahedron	CN/ECoN: 4/	(Fe/Al)–O2 ⁱⁱ	1.938 (5)
	3.903		
As2–O5	1.654 (5)		
As2–O6	1.670 (5)	Tl2 polyhedron	CN/ECoN: 10/
			8.639
As2–O7 ⁱⁱ	1.675 (5)	Tl2–O1 ^{viii}	2.873 (6)
As2–O4 ⁱⁱⁱ	1.770 (5)	Tl2–O1	2.873 (6)
		Tl2–O3 ^{viii}	2.884 (5)
Tl1 polyhedron	CN/ECoN: 8/	Tl2–O3	2.884 (5)
	7.773		
Tl1–O6 ^{vi}	2.854 (5)	Tl2–O5 ^{ix}	2.924 (5)
Tl1–O6	2.854 (5)	Tl2–O5 ^{iv}	2.924 (5)
Tl1–O2 ^{vi}	2.943 (5)	Tl2–O7 ^{vii}	3.275 (5)
Tl1–O2	2.943 (5)	Tl2–O7 ^x	3.275 (5)
Tl1–O7 ^{vii}	3.052 (6)	Tl2–O6 ^{vi}	3.297 (5)
Tl1–O7 ⁱⁱ	3.052 (6)	Tl2–O6 ^v	3.297 (5)
Tl1–O4	3.261 (5)		
Tl1–O4 ^{vi}	3.261 (5)		

Symmetry transformations to generate equivalent atoms: (i) $1-x, -y, 1-z$; (ii) $1-x, 1-y, 1-z$; (iii) $x, 1+y, z$; (iv) $-x, 1-y, 1-z$; (v) $x, y, z-1$; (vi) $-x, -y, 1-z$; (vii) $x-1, y-1, z$; (viii) $-x, -y, -z$; (ix) $x, y-1, z-1$; (x) $1-x, 1-y, -z$.

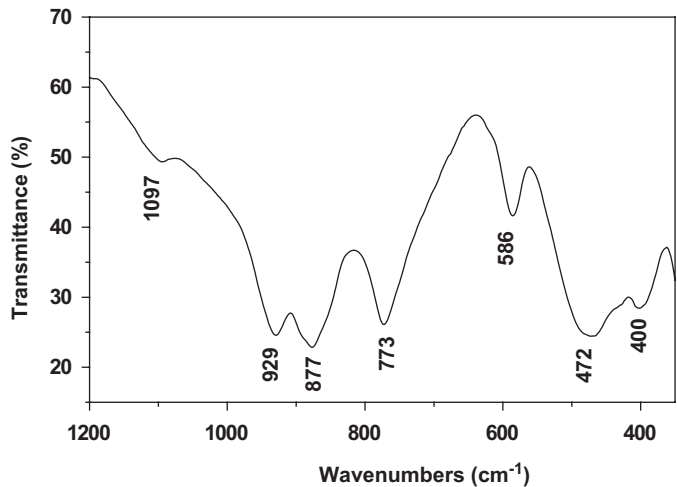


Fig. 3. Infrared analysis spectrum of $TlFe_{0.22}Al_{0.78}As_2O_7$.

400 cm^{-1} . A comparison with data of similar compounds from the literature was used to assign the IR bands [3,20,21].

3.4. Ionic conductivity

Typical complex plots of imaginary part of impedance $-Z''$ versus the real part Z' at various temperatures ($Z^* = Z' - jZ''$) are shown in Fig. 4 in which semicircles are observed. The centres of these semicircles are depressed below the baseline. The ionic conductivity as function of the temperature has been obtained from the values of intercept of the extrapolated high-frequency semicircles with the real axis. It should be noticed that conductivity in this arsenate is of ionic type; the electronic conductivity in oxides is due to overlapping of non-completely filled d or f orbitals of cations or to electron hopping from aliovalent ions, like Fe^{2+} and Fe^{3+} assisted by an oxygen anion in between. In this case, we would exclude both mechanisms so conductivity should be totally ionic, some electronic could be present in grain boundaries, but negligible.

The conductivity variation indicates an increase of conductivity with rise in temperature with a typical Arrhenius-type behaviour having linear dependence of thermal conductivity logarithm $\log(\sigma T)$ on inverse of temperature $10^3/T$ (K^{-1}) (Fig. 4). This type of temperature dependence of the conductivity indicates that the electrical conduction in the material is a thermally activated process. It can be explained in accordance with the expression: $\sigma T = A_0 \exp(-E_a/kT)$, where A_0 is the pre-exponential factor, E_a the activation energy, T the absolute temperature and k the Boltzmann constant. The conductivity value is $5.23 \times 10^{-6} \text{ S cm}^{-1}$ at 683 K and the ionic jump activation energy is 0.656 eV . This material shows a weak ionic conductivity performance, as compared to similar iron arsenates [3]. This will be related to structural features and may be explained by other unfavourable factors.

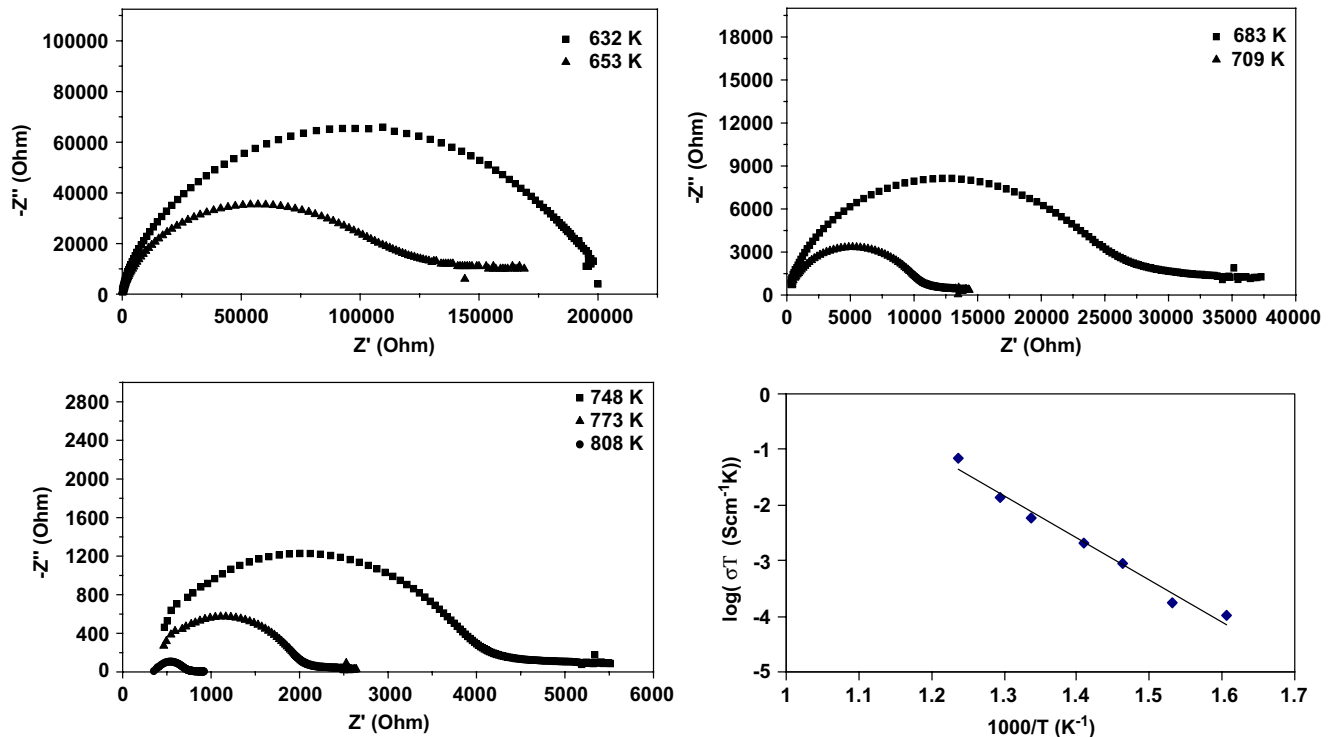


Fig. 4. Complex impedance diagrams $-Z''$ vs. Z' for $\text{TiFe}_{0.22}\text{Al}_{0.78}\text{As}_2\text{O}_7$ over the temperatures ranges 623–653, 683–709 and 748–808 K and Conductivity plot $\log(\sigma T) = f(10^3/T)$.

3.5. Conduction pathway proposed from bond valence analysis

The concept of bond valence [10,11] usually used to validate crystal structures was successfully employed to model lithium ion conductivity in $\text{La}_{2/3-x}\text{Li}_{3x}\text{TiO}_3$ [22] and sodium in Nasicon conductors [23] and in $\text{Na}_2M_2(\text{BO}_3)_2\text{O}$ ($M = \text{Al, Ga}$) and $\text{Na}_{2-2x}\text{Ca}_x\text{Ga}_2(\text{BO}_3)_2\text{O}$ ($x = 0.25, 0.50$) [24]. This model is applied here to the arsenate under investigation in order to predict the Tl(1) and Tl(2) thallium motions in the crystal bulk.

Bond valence sum $\phi(x, y, z)$ is calculated for a grid of points (x, y, z) taking into account that the starting positions for Tl(1) and Tl(2) are the crystallographic positions (1b and 1a, respectively) determined by X-ray diffraction analysis and that the free motion occurred along initial migration directions such as [100], [110] or [001] towards crystallographic sites, following the lowest bond valence sum $\phi(x, y, z)$. Points in this valence map with the lowest ϕ values correspond to stable positions; the highest values are associated with bottlenecks.

The $\text{Tl}(1) \rightarrow \text{Tl}(2)$ and $\text{Tl}(2) \rightarrow \text{Tl}(1)$ motions appear to be easier only for the initial migration direction [001] (Fig. 5). Along this direction, the maximum $\phi(d)$ values (called hereinafter Vumax) are $\phi(d) = 1.20$ and the minimum values are $\phi(d) = 0.85$ for Tl^+ cations along the pathway from Tl(1) to Tl(2) and to Tl(1) again. Along a and b cell directions, the ion motion seems difficult: Vumax = 1.40

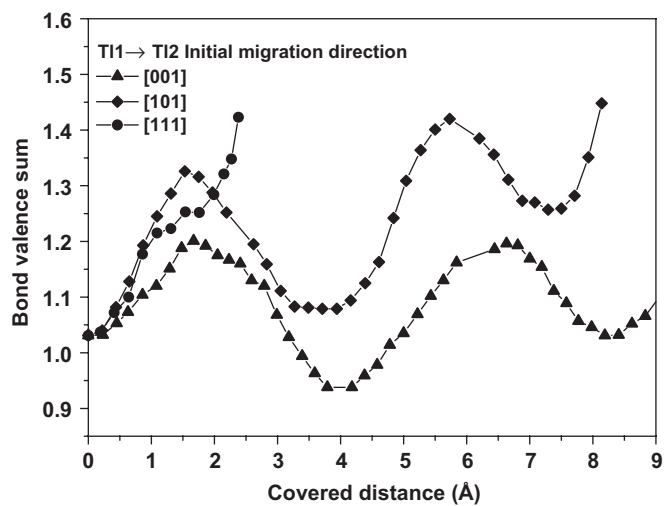


Fig. 5. Bond valence sum for thallium ions versus the covered distance.

for the both cations. The reasons are the dimensions of the tunnels sections for which the largest are those of the tunnels parallel to c -axis (5.27 and 6.296 Å). The conduction mechanism involves a transfer of thallium ions from their crystallographic sites to next ones (1b to 1a in the Tl(1) conduction array). The hopping length of 4.094 Å can be compared with the distance of 4–5 Å found in idealized rhombohedral Nasicon for sodium conduction pathways [23,25]. Then it can be concluded that the Tl^+ ion

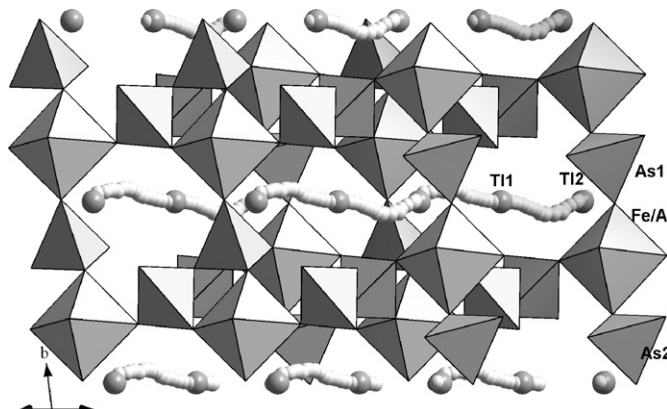


Fig. 6. Schematic representation of the thallium conduction pathways along the [001] direction.

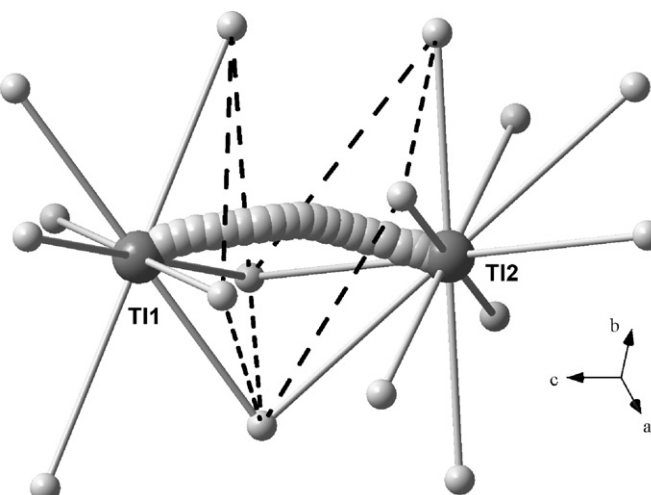


Fig. 7. Optimized trajectory for Tl(1)–Tl(2) jump.

conductivity is mono-dimensional with one path along the *c* direction (Figs. 6 and 7).

4. Conclusion

The crystal structure of the title compound has been elucidated by X-ray crystallography and confirmed by EDS and IR. Bond valence analysis seems to be an important tool to model ionic conduction pathways; performed on $\text{TlFe}_{0.22}\text{Al}_{0.78}\text{As}_2\text{O}_7$, the BVS model reveals that the

thallium ionic conductivity is probably mono-dimensional, mobile along the *c* direction.

References

- [1] J. Belkouch, L. Monceaux, E. Bordes, P. Courtine, Mater. Res. Bull. 30 (1995) 149–160.
- [2] J. Belkouch, B. Taouk, L. Monceaux, E. Bordes, P. Courtine, G. Hechquet, Stud. Surf. Sci. Catal. 82 (1994) 819–822.
- [3] N. Ouerfelli, M.F. Zid, T. Jouini, A.M. Touati, J. Soc. Chim. Tunisie 6 (2004) 85–97.
- [4] S.L. Wang, C.H. Wu, S.N. Liu, J. Solid State Chem. 113 (1994) 37–40.
- [5] CAD-4 Express Software. Enraf-Nonius, Delft, The Netherlands, 1994.
- [6] A.C.T. North, D.C. Phillips, F.S. Mathews, Acta Crystallogr. A 24 (1968) 351–359.
- [7] G.M. Sheldrick, SHELXS-97 A Program for Crystal Structure Determination, University of Göttingen, Germany, 1997.
- [8] G.M. Sheldrick, SHELXL-97 A Program for the Refinement of Crystal Structures, University of Göttingen, Germany, 1997.
- [9] L.J. Farrugia, J. Appl. Crystallogr. 32 (1999) 837–838.
- [10] I.D. Brown, Phys. Chem. Miner. 15 (1987) 30–34.
- [11] Softbv web page by Pr. Stefan Adams: <<http://kristall.uni.mki.gwdg.de/softbv>>.
- [12] R. Hoppe, S. Voigt, H. Glaum, J. Kissel, H.P. Muller, K. Bernet, J. Less-Common Met. 156 (1989) 105–122.
- [13] M. Nespolo, CHARDT-IT A Program to Compute Charge Distributions and Bond Valences in Non-molecular Crystalline Structures, LCM3B, University Henri Poincaré Nancy I, France, 2001.
- [14] M. Nespolo, G. Ferraris, G. Ivaldi, R. Hoppe, Acta Crystallogr. B 57 (2001) 652–664.
- [15] K. Brandenburg, M. Berndt, Diamond Version 2.1, Crystal Impact, Bonn, 2001.
- [16] H. Boughzala, A. Driss, T. Jouini, Acta Crystallogr. C 49 (1993) 425–427.
- [17] H. Boughzala, T. Jouini, Acta Crystallogr. C 51 (1995) 179–181.
- [18] K.J. Lin, K.H. Lii, Acta Crystallogr. C 52 (1996) 2387–2389.
- [19] K. Schwendtner, J. Alloy Compd. 421 (2006) 57–63.
- [20] T. Mihajlović, E. Libowitzky, H. Effenberger, J. Solid State Chem. 177 (2004) 3963–3970.
- [21] R. Hubin, Spectrochim. Acta Pt. A: Mol. Spectrosc. 27 (2) (1971) 311–319.
- [22] D. Mazza, S. Ronchetti, O. Bohnké, H. Duroy, J.L. Fourquet, Solid State Ion. 149 (1–2) (2002) 81–88.
- [23] D. Mazza, J. Solid State Chem. 156 (2001) 154–160.
- [24] G. Corcel, D. Mazza, O. Bohnké, M. Leblanc, Solid State Sci. 7 (2005) 588–593.
- [25] F. Sanz, C. Parada, J.M. Rojo, C. Ruiz-Valero, R. Saez-Puche, J. Solid State Chem. 145 (1999) 604–611.